



Cyano group modified carbon nitride with enhanced photoactivity for selective oxidation of benzylamine



Hao Tan^{a,b}, Xianmo Gu^a, Peng Kong^a, Zan Lian^c, Bo Li^{c,*}, Zhanfeng Zheng^{a,*}

^a State Key Laboratory of Coal Conversion, Institute of Coal Chemistry, Chinese Academy of Sciences, Taiyuan, 030001, China

^b University of Chinese Academy of Sciences (UCAS), Beijing, 100049, China

^c Shenyang National Laboratory for Materials Science, Institute of Metal Research, Chinese Academy of Sciences, Shenyang, 110016, China

ARTICLE INFO

Keywords:
Cyano group
Carbon nitride
Midgap state
Benzylamine
Thin-layered structure

ABSTRACT

Polymeric graphitic carbon nitride ($\text{g-C}_3\text{N}_4$) is a promising photocatalyst but suffers from the high recombination rate of photogenerated carriers. Many strategies for introducing active “sites”, such as heteroatom doping and defect creation, which can hinder recombination by capturing the separated electrons or holes, have been developed to solve the problem. As a polymeric organic material, it is possible to alter the electron structure and improve the charge separation by introducing organic groups with different electronegativities or conjugation properties to the side chains. Herein, we report a facile and efficient $-\text{C}\equiv\text{N}$ group modification strategy using the thermal condensation of the thiocyanuric acid (TA) precursor. The sulfur content in the precursor forms $-\text{C}\equiv\text{N}=\text{S}$ and then transforms to $-\text{C}\equiv\text{N}$. The $-\text{C}\equiv\text{N}$ group introduced catalyst exhibits enhanced light absorption and a low carrier recombination rate based on optical and photoelectrical measurements. This is due to the formation of a $-\text{C}\equiv\text{N}$ group related midgap state between the bandgap of $\text{g-C}_3\text{N}_4$, according to a density functional theory (DFT) calculation. The $-\text{C}\equiv\text{N}$ groups can also loosen the stacking texture of $\text{g-C}_3\text{N}_4$ and result in a thinner layer structure during the post-thermal treatment, which can shorten the distance of photogenerated carrier transfer from the bulk to the surface. The $-\text{C}\equiv\text{N}$ group introduced photocatalyst is efficient for the selective oxidation of benzylamine to imine, even under green light irradiation. This result demonstrates that the introduction of an electron rich conjugation group such as $-\text{C}\equiv\text{N}$ into the edge chain of polymeric carbon nitride is efficient for better photoactivity.

1. Introduction

Photochemical catalysis has received an increasing amount of attention because the global energy and resource shortage requires development of a greener catalytic route to minimize energy consumption and catalyst cost [1–5]. Recently, a class of metal-free photocatalysts consisting of stable photocatalysts from lightweight and abundant elements, including elemental boron, sulfur and phosphorus, such as the polymeric carbon nitride (C_3N_4) [6], has emerged. C_3N_4 is probably one of the most promising photocatalysts due to its advantageous properties such as nontoxicity, thermal/chemical stability, low cost and abundance. C_3N_4 can absorb visible light to offer a sustainable path for hydrogen production [3,7,8], solar energy conversion [9,10] and organic photosynthesis [11–13]. However, the bulk graphitic carbon nitride ($\text{g-C}_3\text{N}_4$) still faces unsatisfactory photocatalytic efficiency due to its fast recombination rate of photogenerated charge carriers, small surface area (approximately $10 \text{ m}^2 \text{ g}^{-1}$) and poor sunlight usage rate (it

only absorbs wavelengths below 470 nm) [14,15]. It is highly desirable to devise a new strategy to solve these problems and improve the photocatalytic performance of carbon nitride.

The catalytic properties of a material are in principle determined by the material's electronic structure. Therefore, changing the charge/spin distribution, especially in the surface electronic structure, can radically change the catalytic performance [16,17]. In addition, a change in the original structure can directly influence the electronic properties of materials. For this reason, various modification approaches such as doping with metal/nonmetal ion atoms [18–20], designing nanostructure through inorganic or organic templates [21–23], forming carbon nitride heterojunctions [24,25], dye sensitization [26] and thermal or other exfoliation methods [15,27,28] have been used to improve the photocatalytic properties of C_3N_4 catalysts. Unlike doping or the defect-producing methods, using the edge effects or edge sites to promote catalytic properties can also be considered a promising approach (e.g., edge-halogenation, which can benefit the charge transfer

* Corresponding authors.

E-mail addresses: boli@imr.ac.cn (B. Li), zfzheng@sxicc.ac.cn (Z. Zheng).

and favorable substrate adsorption) [17,29]. A recent study indicates that the cyanamide moiety can improve the separation of the photo-excited charges by built-in electrostatic potential differences [30]. Screening of new methods for organic group doping and understanding the mechanism is of great importance towards the improvement of photoactivity. The selective photocatalytic oxidation of benzylamine and its derivatives to corresponding imines has attracted an enormous amount of attention, because imines are important intermediates for the synthesis of fine chemicals and pharmaceuticals and this reaction can endow room temperature synthesis with molecular oxygen and metal-free catalyst under renewable solar light irradiation [12,31].

In this study, we design a simple and effective method to achieve $-C\equiv N$ group modification of C_3N_4 . The sulfur-containing compound trithiocyanuric acid was used to introduce the $-C\equiv N$ groups. The sulfur in trithiocyanuric acid plays a significant role in assisting the generation of the $-N=C=S$ intermediate group, with the subsequent release of SO , SO_2 or CS_2 to form a $-C\equiv N$ group. We explored the polymerization steps at the molecular level and presented the detailed sulfur removal and $-C\equiv N$ group generation process. The attachment $-C\equiv N$, which has diverse hybrid forms, can tailor the original electronic band structure of carbon nitride. Various reports including nitrogen modification or doping of rf plasma deposited carbons prove that the change of hybrid form can have a large influence on the electrical properties of the material [32–34]. The experimental and the density functional theory (DFT) results show that the sp hybrid structure can redistribute the charge and create a mid-bandgap and then enhance the light usage efficiency. The $-C\equiv N$ groups can tune the stacking structure of carbon nitride and favor the production of a thin layer structure by thermal treatment. After the above treatment procedure, the catalyst exhibits high activity and selectivity for oxidizing benzylamine and its derivatives at room temperature.

2. Experimental

2.1. Preparation of catalysts

2.1.1. Bulk $g-C_3N_4$ (designated as CN)

In a typical synthesis, 10 g of melamine was heated at 550 °C with a ramping rate of 3 °C min⁻¹ for 4 h.

2.1.2. $-C\equiv N$ introduced C_3N_4 (CNS or CNS-*n*)

A cyano group introduced sample was prepared by thermal treatment of the mixture of trithiocyanuric acid (TA), and melamine (**Scheme 1**). Specifically, *n* g of trithiocyanuric acid (TA), and *m* g of melamine (*n* + *m* = 10 g) were dissolved in ethanol and dried thoroughly to get a yellow block mixture. The mixture was heated through the above calcination procedure. Because the preliminary studies showed that CNS with a mass ratio TA:(TA + melamine) of 0.75:1 provides the highest conversion of oxidation reaction (Fig. S1), this mass ratio was chosen for the current study.

2.1.3. Post-thermal treatment (TCNS or TNCS-*xh*)

Typically, 300 mg of CNS in a porcelain boat was heated in an argon atmosphere in a tube furnace for 1, 2, 4 and 8 h (named as TCNS-1 h,

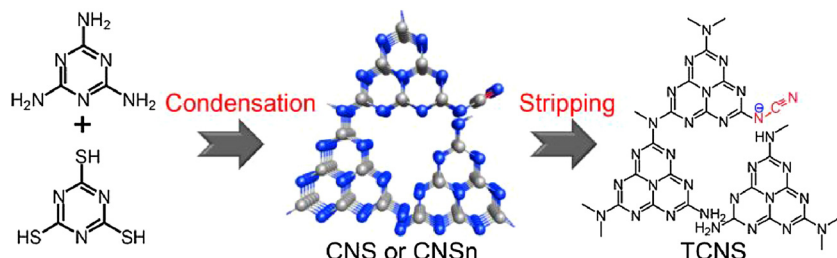
TCNS-2 h, TCNS, TCNS-8 h, respectively). The 4 h thermal stripping sample was chosen for the current study and the detailed catalyst screening process is shown in the supporting information (SI, Fig. S2).

2.2. Sample characterization

Powder X-ray diffraction (XRD) spectroscopy was performed on a Bruker D8 Advanced diffractometer operating with Cu $K\alpha_1$ radiation ($\lambda = 1.5405 \text{ \AA}$). The morphology was operated using transmission electron microscopy (TEM, Tecnai G2 F20 S-Twin) with an accelerating voltage of 200 kV. Atomic force microscopy (AFM) analysis was conducted on a Bruker Dimension Icon instrument. Fourier transformed infrared (FTIR) spectra were obtained on a Nicolet Magna-IR 550-II spectrometer using KBr as a standard reference sample, and the mass ratio between KBr and the sample was 50:1. The surface area was obtained on a TriStar II 3020 using the Brunauer–Emmett–Teller (BET) method and measurement at –196 °C in nitrogen. Prior to the measurement, all the photocatalysts were degassed under evacuation at 150 °C for 10 h. The pore size distribution was obtained by desorption isotherms using the Barret–Joyner–Halender (BJH) method. Thermogravimetric analysis (TGA) was characterized on a Thermo Plus EVO at a ramping rate of 10 °C min⁻¹ in the air atmosphere using Al_2O_3 as a reference. The UV-vis diffuse reflectance spectra (DRS) were observed on a Shimadzu UV-3600 UV-vis-NIR spectrophotometer using $BaSO_4$ as a reference and the diffuse reflectance accessory. Element analyses (EA) for carbon and nitrogen were collected from a Vario EL III element analyzer. Photoluminescence (PL) spectra were performed on a Hitachi F-7000 FL spectrophotometer at room temperature with an excitation wavelength of 365 nm. Electron paramagnetic resonance (EPR) measurements were obtained using a Bruker model EMXPLUS 10/12 spectrometer. X-ray photoelectron spectroscopy (XPS) data were obtained on a USA Thermo ESCALAB 250 with a monochromatized Al Ka line source (200 W). The binding energy correction was referenced to C 1s peaks (284.8 eV) arising from surface hydrocarbons.

2.3. Photoelectrochemical measurements

Electrochemical tests [transient photocurrent (TP), Mott–Schottky plots and electrochemical impedance spectroscopy (EIS)] were characterized on a workstation (CHI 760D, CH Instruments, Inc., Shanghai, China) coupled with a PINE rotating disk electrode (RDE) system (from Pine Instruments Co. Ltd. USA) in a three-electrode model. A Ag/AgCl electrode (saturated KCl) was used as a reference electrode and Pt wire was used as the counter electrode. Before measurement, the working electrode was prepared as follows: 5 mg of the catalyst powder was mixed with 0.5 g of 2 wt.% polyvinylidene difluoride (PVDF) *N*-methyl pyrrolidone (NMP) solution, and then, ultrasonication was performed until a homogeneous mixture was obtained. Finally, 20 μL of the slurry was spread onto the fluorine-doped tin oxide (FTO) glass electrode. The TP measurements were performed under illumination conditions and the working electrodes were immersed in 0.2 M Na_2SO_4 aqueous solution with the pH maintained at 6.8. Mott–Schottky plots were obtained using the impedance-potential technique with the working electrodes immersed in 0.2 M Na_2SO_4 aqueous solution. The electrochemical



Scheme 1. Illustration of the preparation process for cyanide modified thin-layered C_3N_4 .

impedance spectra (EIS) were also obtained on the abovementioned three-electrode system. For the oxygen reduction reaction (ORR) test the glass carbon coated with the electrocatalyst was used as the working electrode. To prepare the working electrode, the catalyst ink was prepared by ultrasonically dispersing 5 mg of catalyst in a 1 mL mixture of ethanol and Nafion (DuPont, 5 wt.%) (volume ratio = 8:2) to form a homogeneous suspension. Then, 10 μ L of ink was dispersed onto a glassy carbon rotating disk electrode (RDE, 5 mm diameter, Pine Instrument Co.) and dried thoroughly in air for 12 h.

2.4. Photoactivity measurements

The benzylamine oxidation reactions were conducted under an O_2 atmosphere (1 atm) in a 10 mL round-bottom Pyrex glass flask with a sealed spigot and a magnetic stirrer. The concentration of benzylamine was 0.1 M using LED white light as the light source. The products were analyzed and determined using a GC–MS spectrometer (Agilent HP5973).

2.5. Computational setup

All calculations were performed using Gaussian 09 code [35]. All structure optimizations were performed at the PBE/6-31G* level and each optimized structure was verified to be a local minimum by a frequency calculation. The energy and density of states were further refined at the HSE06/6-31G** level.

3. Results and discussion

3.1. Identification of cyano group ($-C\equiv N$) in C_3N_4 structure

The samples CN, CNS and TCNS were analyzed using FT-IR spectroscopy (Fig. 1a). All three samples show a sharp absorption band at 810 cm^{-1} , which is recognized as the typical breathing vibration of the triazine units of C_3N_4 [36]. The absorption at 1200–1600 cm^{-1} is the stretching vibration of $-C-N$ heterocycles and the broad band at 2900–3400 cm^{-1} is ascribed to the $-OH$ stretching band of absorbed H_2O molecules and the $-NH_2$ stretching vibration of uncondensed amine groups [37–39]. An obvious new absorption band at 2100–2250 cm^{-1} was observed for the CNS and TCNS samples, which can be attributed to the $-C\equiv N$ groups [40–43], whereas no peak was detected in this range for the CN sample. Moreover, a gradually enhanced absorption band of the $-C\equiv N$ group was observed when the proportion of TA was increased. These results demonstrate that the trithiocyanuric acid precursor is effective for introducing the cyano group into the CN heterocycles (Fig. S3a). The stripping samples TCNS and TCNS-x exhibit a similar $-C\equiv N$ group peak intensity (Fig. S3b), suggesting that the $-C\equiv N$ group is stable existence in the sample. The contents of the $-C\equiv N$ groups in the CNS and TCNS samples were determined using 4-nitrobenzonitrile and the CN sample as references to draw a standard curve (the detailed calculation is shown in Fig. S4 and the relevant results are shown in Table S1) as a function of the cyano intensity in the IR spectra. According to the standard curve, the contents of the cyano groups in the CNS and TCNS samples were 5.5 wt.% and 4.5 wt.%, respectively.

The $-C\equiv N$ group introduction process using trithiocyanuric acid as a precursor was monitored using TG–MS, IR and XRD analysis. As shown in Fig. 1b, the condensation process can be divided into two stages. The first stage and the second stage occurred at approximately 200 °C and 300 °C with approximately 24.8% and 66.0% of the weight loss, respectively. According to the result, trithiocyanuric acid was calcined at temperatures from 150 to 550 °C. For the sample calcined at 250 °C, the (002) peak in the XRD pattern (Fig. S5) and the triazine ring vibration peak in the IR spectrum (Fig. 1c) were observed, which implies the occurrence of preliminary polymerization. Meanwhile, a small amount of H_2S was detected, due to the formation of compound (2)

(Fig. 1d) with the release of one molecule of H_2S . When the temperature exceeded 300 °C, all $-C-S$ peaks (460 cm^{-1} in FT-IR spectra) [44] disappeared (Fig. 1c) and the main polymerization process emerged. The fragments of trithiocyanuric acid and the dicyandiamide (3) were subsequently detected by TG–MS (Fig. S6), which may generate dicyandiamide by intermolecular recombination. According to a previous study, dicyandiamide is the precursor for the synthesis of melamine (4) [37], which indicates that dicyandiamide is one of the important intermediates for the condensation reaction. After the generation of melamine (4), two possible paths were triggered. One is the self-polymerization of melamine (4) to form compounds (5) and (6) and finally produce one of the basic composition unit compounds (7). In addition, melamine (4) can also condense with trithiocyanuric acid (1) to form compound (8). We suspect that the downstream product of (8) should condensate with compound (7) to proceed to the next step of polymerization. The dark yellow line in Fig. 1c (TA-250: trithiocyanuric acid as a precursor after thermal treatment at 250 °C for 4 h) implies the formation of a $-N=C=S$ group [45,46]. The probable framework of compound (9) is provided in Fig. 1d. Compound (9) can form another unit (10), and it can condensate with (7) to form compound (11). When the temperature exceeded 350 °C, almost all the sulfur species were released and the $-C\equiv N$ group was finally introduced via the formation process shown in detail in Fig. S7. The structure of $-C\equiv N$ group modification sample is shown as compound (12). Notably, no obvious sulfur signal was observed (Fig. S8a and b) by applying X-ray photoelectron spectroscopy (XPS) to CN, CNS and TCNS samples, indicating that all the sulfur content is released from the structure. Therefore, the condensation process of trithiocyanuric acid can be tuned by the sulfur species. The released components such as H_2S , SO_2 , and CS_2 (detected using TG–MS, Fig. S9a–c), can act as the foaming agent and loose the stacking structure. The SCN[−] fragment (Fig. S9d) is formed in the pyrolysis of trithiocyanuric acid and can react with the $-N=C=S$ group to form the final cyano group (Fig. S7).

The unique crystal structure change forces us to evaluate the thermal stability of carbon nitride polymers of all samples using thermogravimetric/differential thermal analysis (TG/DTA) methods (Fig. S10). The $-C\equiv N$ group modification samples showed lower thermal stability than the original carbon nitride. The triazine units are stacked together through hydrogen bonds between the strand nitrogen atoms and terminal NH/NH₂ groups [47]. The $-C\equiv N$ group can alter the above stacking pattern and decrease the thermal stability of CNS and TCNS, which provide the prerequisites for obtaining a thinner structure via the thermal treatment method.

3.2. Physical properties (crystal structure, optical property and band structure) changes after $-C\equiv N$ group introduction

All prepared carbon nitride samples exhibit lamellar structure from TEM observation. The thickness of the CNS sample is 50–60 nm, much thinner than a particle of the CN sample (100–120 nm, melamine as a precursor) from TEM and AFM analysis (Fig. 2a and b). This further confirms that the $-C\equiv N$ group can alter the stacking pattern and favor the production of a thinner structure besides the gases released from TA can altered the connectivity patterns and topology of the condensed graphitic carbon nitride sheets [48]. In addition, the TCNS sample (10–15 nm, further thermal treatment of CNS at 550 °C for 4 h) exhibits a porous structure (Fig. 2c). As shown in Fig. 2d and Table S2, TCNS presents the largest pore volume (0.14 $cm^3 g^{-1}$) and surface area (67.6 $m^2 g^{-1}$) among the three samples. These data agree well with the $-C\equiv N$ group introduction process. On the one hand, the sulfur can *in situ* tune the polymerization path. On the other hand, the selective breaking of hydrogen bonds can produce porous in the carbon nitride [49], once the terminal NH/NH₂ groups replaced by $-C\equiv N$ group, it can also break the hydrogen bonds, thus creating a more porous structure. The structure with a large surface area will have more reaction sites, which increases the probability of physical and chemical

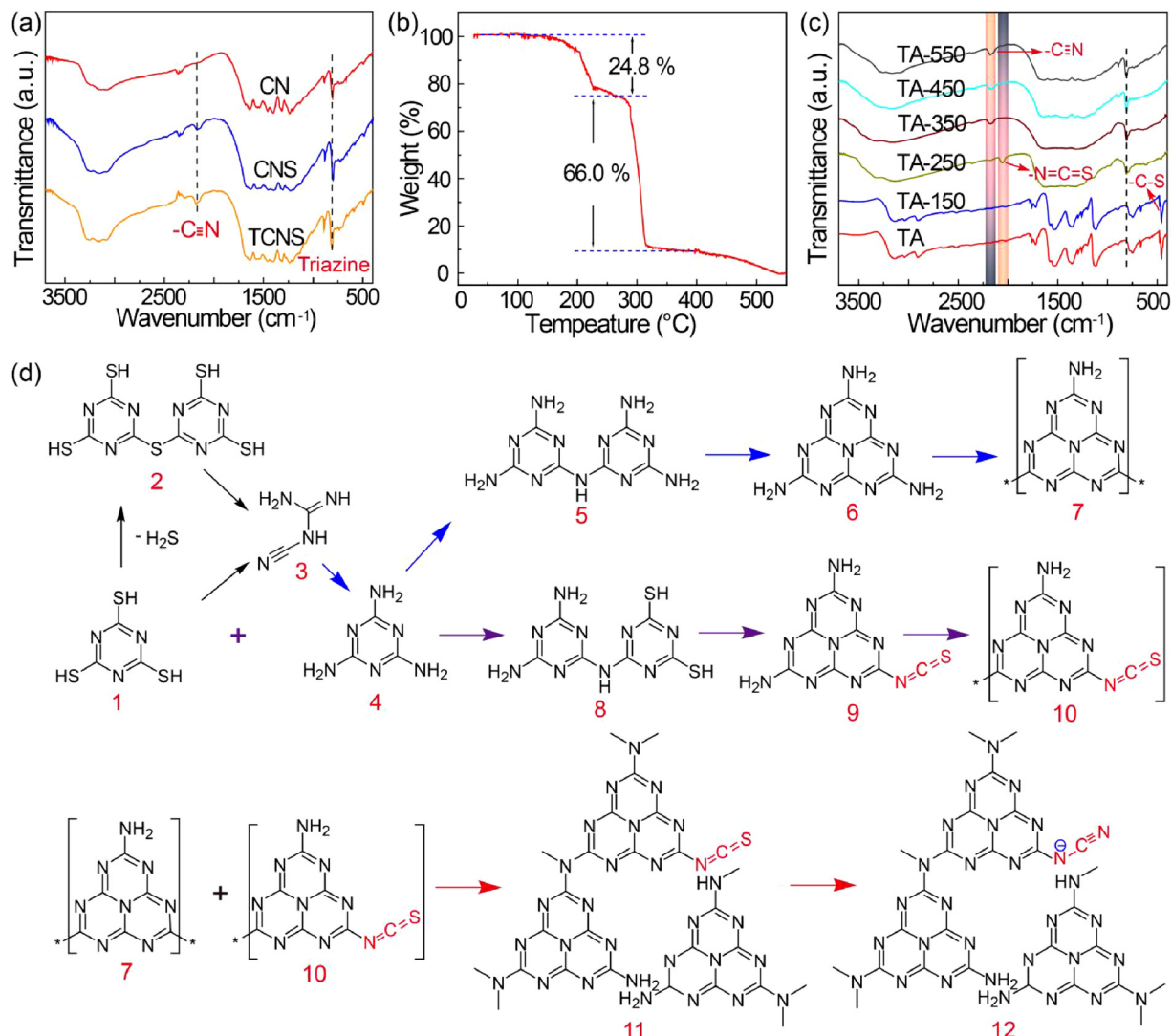


Fig. 1. Proposed $-\text{C}\equiv\text{N}$ group introduction mechanism. (a) FT-IR patterns of samples CN, CNS and TCNS. (b) TG curves of the condensation process of trithiocyanuric acid (TA) in air at a heating rate of 3 K min^{-1} . (c) FT-IR patterns for TA calcined at different temperatures. (d) Proposed formation process of $-\text{C}\equiv\text{N}$ group introduction sample.

adsorption of substrates [50].

The distance between two layers can affect the hybridization of layer atoms and may affect the transfer efficiency of photoinduced carriers [51,52]. The stacking structure change due to $-\text{C}\equiv\text{N}$ modification is measured using X-ray diffraction (XRD) spectroscopy. CNS and TCNS samples exhibit lower intensity than that of the CN sample, which indicates that the $-\text{C}\equiv\text{N}$ containing samples have poorer crystallinity than the CN sample (Fig. 2e and f). The typical interlayer-stacking (002) peak at 27.47° ($d_{002} = 0.324 \text{ nm}$) and the in-plane peak (100) at 12.86° ($d_{100} = 0.688 \text{ nm}$) were observed for CN. However, the (100) peak in the CNS and TCNS samples is shifted to 12.80° ($d_{100} = 0.691 \text{ nm}$) (Fig. 2f) which indicates that the void to void distance increased after introducing the cyano group [38,39]. Meanwhile, the (002) peak of CNS and TCNS was slightly shifted to 27.60° ($d_{002} = 0.322 \text{ nm}$, Fig. 2f), implying the decrease of the interlayer-stacking distance of CNS. In addition, the main interlayer and in-plane structure remain unchanged after the post thermal treatment. The optical absorption and bandgap change caused by $-\text{C}\equiv\text{N}$ introduction were measured using UV-vis diffuse reflectance spectroscopy (Fig. 3a) and Mott-Schottky plots (Fig. 3b). The bandgap (E_g) energies for the CN and CNS samples, 2.74 and 2.66 eV, respectively, were calculated using the Kubelk-Munk equation (Fig. S11a and b) [53]. For TCNS, with

weak crystallinity and a porous structure, a slight blueshift of the absorption was observed and the bandgap was approximately 2.70 eV (Fig. S11c). Usually, the low crystallinity and porous structure will cause a hypsochromic shift of the absorption edge in the UV-vis spectra as a result of delocalization of the π -conjugation system or the quantum confinement effect [54,55]. The electrochemical Mott-Schottky curve indicates a typical n -type plot for all samples, and provides values of the flat band potential at -1.25 eV , -1.07 eV and -1.04 eV vs. Ag/AgCl, which correspond to -1.03 eV , -0.85 eV and -0.82 eV vs. SHE for CN, CNS and TCNS, respectively. The $\text{O}_2^{\cdot-}$ radical redox potential is -0.33 V (vs. SHE) [56], which indicates that all sample can convert the O_2 to $\text{O}_2^{\cdot-}$ radicals under bandgap excitation. In addition, the $\text{PhCH}_3\text{NH}_2^+$ radical redox potential is 0.13 V (vs. SHE) [57], indicating all sample can oxidize the benzylamine (Fig. 3c).

After $-\text{CN}$ group introduction, CNS and TCNS showed a strong Urbach tail absorption in the visible light region, which gives a significantly lower energy gap of 2.07 and 2.11 eV, respectively (Figs. 3c and S11). To further investigate the influence of the added $-\text{CN}$ group, DFT calculations were performed. C_3N_4 and C_3N_4 attached with one $-\text{CN}$ group were investigated. The optimized structures are shown in Fig. 3g and h (left). A melon pentamer unit is used to represent original C_3N_4 and the effectiveness of this model has been verified in previous

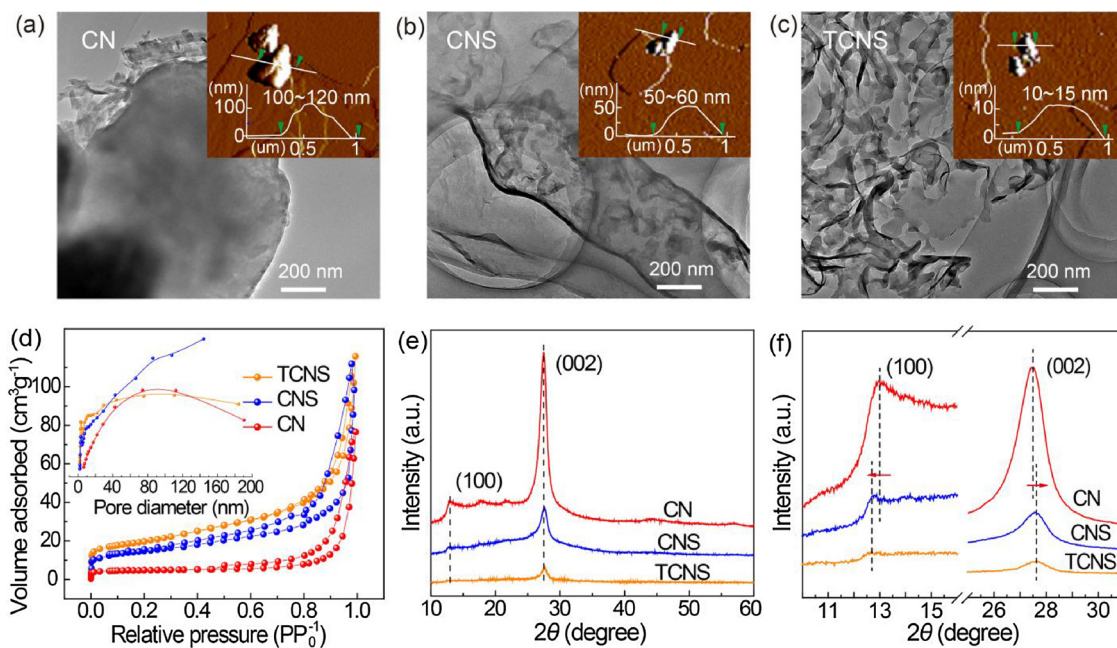


Fig. 2. Crystal structure and morphology characterization. (a–c) TEM image with the inset AMF spectra showing the corresponding height profile of CN, CNS and TCNS. (d) N_2 sorption isotherms with the inset displaying the corresponding pore size distribution curves. (e) XRD patterns and (f) the region of the main peak near 13° and 27° .

studies [30]. The $-\text{CN}$ group is attached at the end of the melon pentamer and the optimized distance between nitrogen and $-\text{CN}$ is 1.3\AA . The most obvious change induced by $-\text{CN}$ is observed in the density of states (DOS) as shown in Fig. 3g and h (right). The bandgap is predicted to be 2.45 eV for original C_3N_4 , and is reduced to 2.11 eV after the introduction of $-\text{CN}$, which conforms to the experimental results. It is clearly indicated that a new state appeared in the gap after $-\text{CN}$ modification. The new state, which is indicated by the red arrow, is slightly above the valence band and filled. Therefore, the $-\text{CN}$ attachment resembles n-doping. The new midgap state substantially reduces the bandgap, which may improve the photocatalytic activities.

According to the DFT calculations, the effect of the sp hybrid $-\text{CN}$ groups at the termini of the sp^2 hybrid CN rings resembles n-doping, and the increasing electron paramagnetic resonance (EPR) signals after $-\text{CN}$ groups introduction further confirm this result (Fig. 3d). Only a single Lorentzian line centering at $g = 2.0034$ was obtained for the CN and $-\text{CN}$ introduced sample CNS. The Lorentzian line is assigned to the unpaired electrons in the sp^2 -carbon in the π conjugated $-\text{C}=\text{N}$ heterocycles [58]. The $-\text{CN}$ group can provide more unpaired electrons and finally increase the EPR signals. After irradiation, the signals of the CN and CNS samples are greatly enhanced, which indicates the efficient generation of electron-hole pairs in the C_3N_4 polymers.

The generation of photoinduced charges and their separation and transfer is deemed the basic process for semiconductor photocatalysts [38]. The photocurrent measurement provides information on the generation and separation efficiency of photoexcited electron-hole pairs in the semiconductor (Fig. S12). The photocurrents of the $-\text{C}\equiv\text{N}$ group modified samples CNS and TCNS are nearly 3- and 5-fold larger than that of sample CN, respectively, due to the increased efficiency of charge generation and separation. The room temperature photoluminescence (PL) spectra predicate the recombination rate of photoexcited carriers [38]. As shown in Fig. 3e, all samples showed emission peaks at $400\text{--}600\text{ nm}$ with the excitation wavelength at 365 nm . Samples CNS and TCNS have a lower intensity signal response than CN. This indicates that the recombination rate of photogenerated electron and hole pairs in the $-\text{C}\equiv\text{N}$ groups containing samples CNS and TCNS is largely impeded. Electrochemical impedance spectroscopy (EIS) measurements were performed in dark ambient conditions to evaluate the

charge separation efficiency of all samples. As shown in Fig. 3f, all samples presented the EIS Nyquist plots. The EIS Nyquist plot is analogous to an electrical equivalent-circuit model similar to the one shown in the inset of Fig. 3f, where R_s represents the electrolyte solution resistance and R_t represents the interfacial charge-transfer resistance [14]. CN has a much larger Nyquist plot diameter than that of CNS and TCNS. We can confirm that our sample preparation method can be regarded as a feasible tactic for improving the charge mobility rate of carbon nitride.

3.3. Correlation of the $-\text{C}\equiv\text{N}$ groups and the enhanced photoactivity

The photocatalytic performances for the selective oxidation of benzylamine to imine using CN, CNS and TCNS as catalysts are summarized in Fig. 4a. All samples exhibited high selectivity ($> 99\%$) for the conversion of benzylamine to imine. The benzylamine conversion rate over TCNS was the highest at 92% , compared to CNS and CN at 71% and 19% , respectively (4 h, detailed reaction conditions shown in the caption of Fig. 4). No imine product was observed in the absence of O_2 or irradiation, which confirms that the oxidation of benzylamine on carbon nitride is a dioxygen oxidation and a light-driven reaction. This is consistent with previous reports using different metal oxide photocatalysts for amine oxidation [56,59].

Generally, the overall photocatalytic efficiency is determined by the efficiency of three elementary processes: light absorption, charge separation, and surface catalytic reactions. As stated in the last section, the introduction of the $-\text{C}\equiv\text{N}$ groups influences the light absorption and charge separation and may be responsible for the good photoactivity of CNS and TCNS. In this part of the study, the detailed surface reactions involving the reaction tempertaure, light intensity, active sites, adsorption and desorption process, etc., are examined carefully to uncover the high activity for the samples with $-\text{C}\equiv\text{N}$ groups.

A large surface area normally has a linear realtionsip with the number of active sites. The specific surface area of TCNS ($67.9\text{ m}^2\text{ g}^{-1}$) is approximately 4.8-fold larger than that of CN ($14.2\text{ m}^2\text{ g}^{-1}$), whereas the conversion rate over TCNS (92%) is approximately 7.6-fold larger than that over CN (12%). It seems that the large surface area should be responsible for the high activity. However, the light absorption should

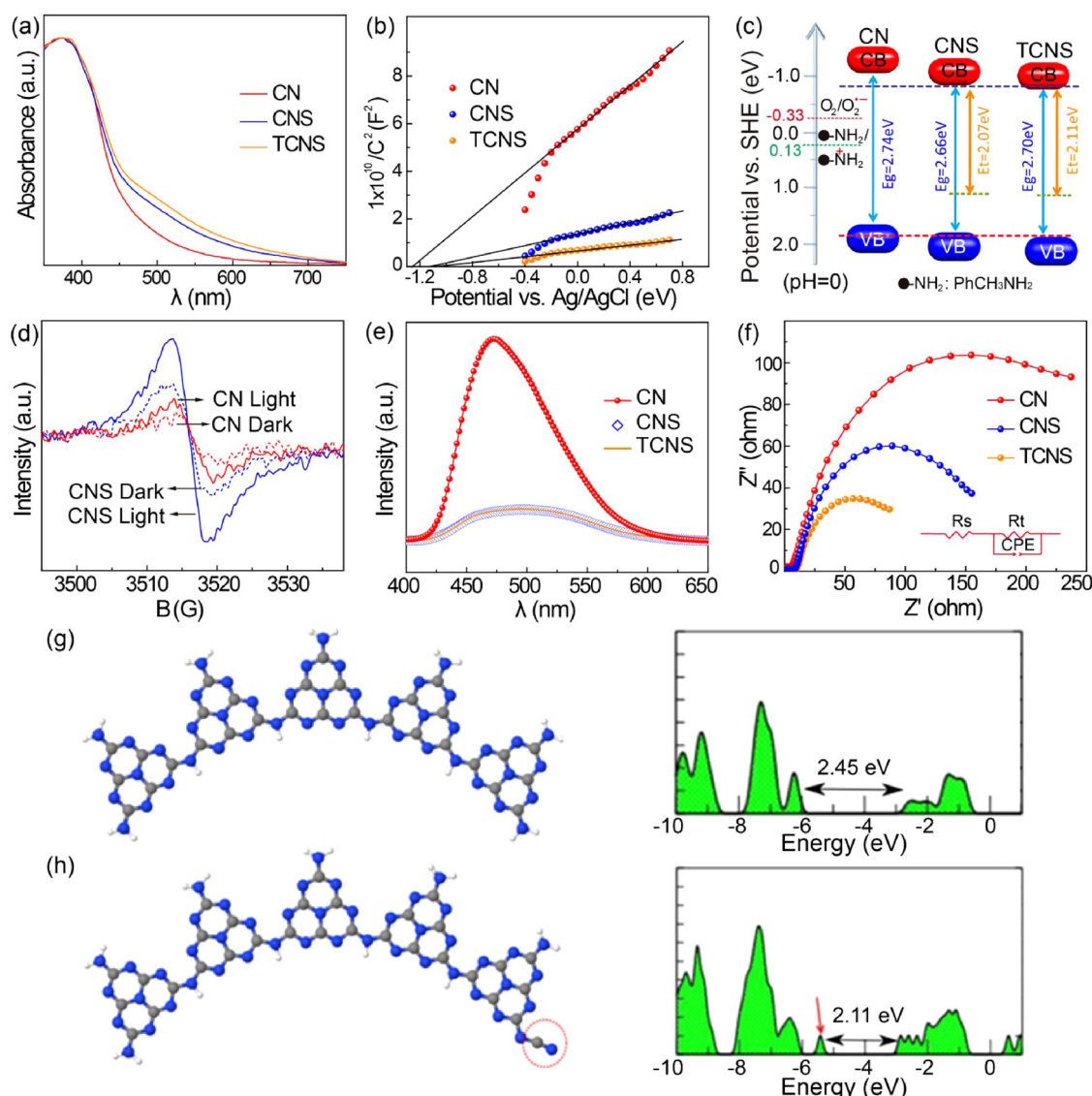


Fig. 3. Optical and electronic properties of CN, CNS and TCNS. (a) Ultraviolet-visible diffuse reflectance spectrum (b) Mott-Schottky plots in 0.2 M Na_2SO_4 aqueous solution. (c) Electronic band structures vs. SHE. (d) Solid state EPR spectra with visible light or in the dark (B = magnetic field strength). (e) PL spectra under excitation wavelength of 365 nm. (f) EIS Nyquist plots measured in 0.2 M Na_2SO_4 aqueous solution. The optimized structures (left) and density of states (right) of (g) C_3N_4 and (h) $-\text{C}\equiv\text{N}$ group modification C_3N_4 .

not be neglected. For the CN and TCNS catalysts, the conversion rate has a linear relationship with the catalyst amount when it is less than 10 mg; however, the conversion rate does not increase with the dosage of catalyst when it exceeds 10 mg (Fig. S13). This result indicates the existence of an optimal threshold value of light usage efficiency, as the excessive catalyst may block other catalyst powders and provide no contribution to the photocatalytic reaction. A control experiment shows that when 2.08 mg of TCNS was used (surface area normalized to that of 10 mg of CN, should have a similar amount of surface sites), 20.5% of benzylamine is converted to imine. Consider that it used only a fraction of the incident light (approximately 21%) compared to that for the 10 mg sample. We can safely conclude that the large surface area of TCNS that is obtained by thermal stripping is important but not decisive for the high activity and that the $-\text{C}\equiv\text{N}$ groups are the key factor. However, to obtain a modified catalyst the enhanced photoelectric properties caused by $-\text{C}\equiv\text{N}$ modification and the increased surface area caused by thermal stripping are essential.

The conversion of benzylamine as a function of temperature over TCNS under visible light irradiation (200 mWcm^{-2}) is shown in Fig. 4b (blue line). The conversion rate of benzylamine increased from 40% to

87% when the reaction temperature was increased from 40 to 100 °C. This is unusual for a semiconductor photocatalyst, for which the charge carrier recombination rate will generally increase with temperature, thus increasing the reaction temperature and decreasing the reaction rate [59]. However, the temperature can affect several aspects of the catalytic reaction. For instance, in a surface catalytic process, if the reaction rate follows an Arrhenius dependence on temperature, then an elevated temperature can accelerate the reaction rate [60]. In this study, for a semiconductor photocatalyst, we propose that the temperature can affect the reaction in two ways. It can affect the excitation of the semiconductor and accelerate the desorption of activated molecules. At 100 °C (in the absence of light), no imine was generated, which indicated that the reaction is not thermally excited. Once the reaction system was irradiated, the yield of imine increased with the temperature, which implies that heat can affect but not excite the reaction. This hypothesis conforms to the photocurrent data at different temperatures, which show that the current density increases with the temperature (Fig. S14). In addition, a higher temperature can promote the desorption rate of activated molecules from the catalyst surface and accelerate the subsequent process [61]. Keeping the other conditions

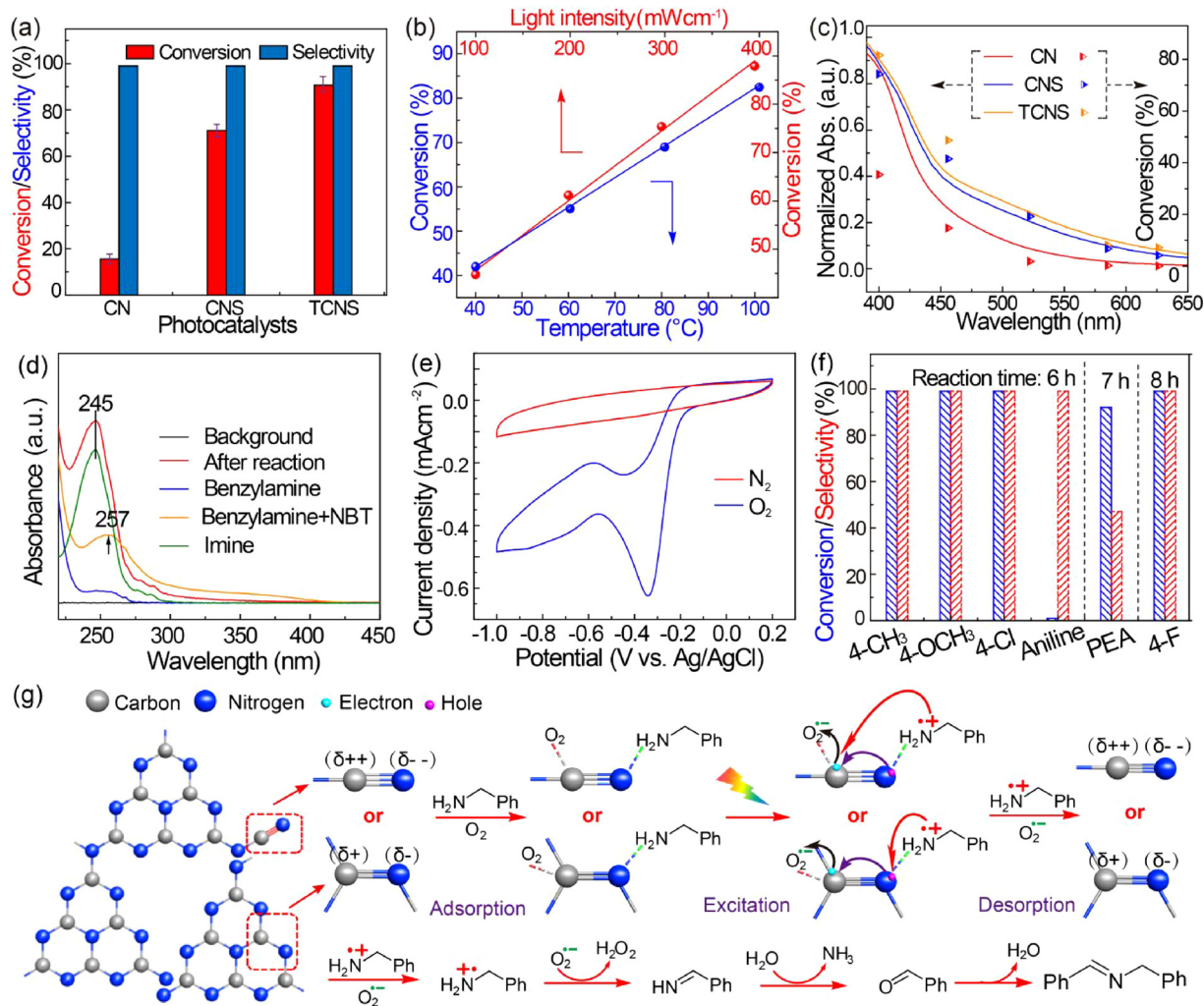


Fig. 4. Performances of CN, CNS and TCNS for the selective oxidation of benzylamine under visible light and a schematic illustration and the mechanism research. (a) Catalytic capability comparison. (b) Performance of TCNS as a function of temperature (blue line react for 1 h) and as a function of light intensity (red line react for 2 h). (c) The conversion of CN, CNS and TCNS as a function of wavelength (purple 400 nm, blue 459 nm, green 525 nm, yellow 580 nm, red 625 nm). (d) UV absorption spectrum of the reaction solution. (e) CV curves in N₂-saturated (red line) and O₂-saturated (blue line) 0.1 M KOH aqueous solutions. (f) Conversion and selectivity for catalytic aerobic couplings of various benzylamines. (g) Proposed reaction mechanism for benzylamine oxidation. Reaction conditions: benzylamine (0.2 mmol), acetonitrile (2 mL), catalyst (10 mg), O₂ (1 atm), 60 °C, LED light. (For interpretation of the references to colour in this figure legend, the reader is referred to the web version of this article.)

identical, the reactions were run in different light intensities at 60 °C, and a higher conversion rate was obtained under enhanced light intensity (Fig. 4b, red line). A higher light intensity provides more incident photons and generates more effective electrons to participate in the reaction.

The influence of irradiation wavelength on the conversion rate was also investigated (Fig. 4c). Five colored LED lights were used to control the wavelength [purple (375–430 nm, center peak at 400 nm), blue (420–510 nm center peak at 459 nm), green (480–600 nm, center peak at 525 nm), yellow (550–610 nm, center peak at 580 nm) and red center peak at 625 nm]; the output spectra are shown in Fig. S15]. The apparent quantum efficiency (AQE) under each wavelength was calculated (Fig. S16). The AQE value varies with the wavelength of irradiation: TCNS exhibits a much higher AQE at the shorter wavelength than the longer wavelength because –C≡N group modified carbon nitride has better light absorption ability at the short wavelength (Fig. 3a). As reported, few photocatalysts can drive photocatalytic reactions under green light [1,62]. As shown in Table S3, after irradiating by green light for 2 h, TCNS (20%) possesses obvious advantages over P25 (1.5%), anatase (1.4%), rutile (0.9%) and WO₃ (0.7%) for synthesizing imine. For a semiconductor photocatalyst, only light with an

energy exceeding the bandgap can trigger the reaction, that mild activity under green light can attribute to the –C≡N groups modification. The mid-bandgap caused by –C≡N groups is 2.11 eV, in which case that condition 588 nm, the green light has enough energy to excite the photoelectron to break through the mid-bandgap. Due to the effect of the mid-bandgap, samples CNS and TCNS can use green light, which effectively broadens the range of usable wavelengths. The oxidation of benzylamine using TNCS was also conducted under sunlight for 7 h (Fig. S17). The mean intensity of the sunlight was 60.1 mWcm⁻² and the ground temperature was approximately 35 °C. A total of 75% of benzylamine was converted to imine with selectivity at 99%, which suggests that it is viable to drive the synthesis of imine using the TCNS photocatalyst with sunlight at ambient temperature.

To understand the trigger of the reaction, a series of control experiments to trap active species were implemented. As discussed above, the 2p orbitals of the carbon atom comprise the CB structure, O₂ is adsorbed by the carbon atom and captures the photoelectron to be reduced to O₂·⁻, and the nitroblue tetrazolium (NBT) exhibiting an absorption maximum at 257 nm is used to capture the O₂·⁻ generated by the catalyst. As shown in Fig. 4d after the reaction the main peak at 257 nm disappeared and a new peak at 245 nm that we identify as an

imine was observed on a UV-vis spectrophotometer. Meanwhile, the conversion rate decreased when we added the NBT (Fig. S18a). This indicates that O_2^{+} is generated during the reaction. Moreover, the conversion rate increased with the oxygen pressure (Fig. S18b), but O_2 alone cannot drive the oxidation reaction, it must be reduced to O_2^{+} by capturing the photogenerated electron to activate itself. $AgNO_3$ can be used as a fine electron trapping agent, and once it was added to the reaction system the yield of imine decreased precipitously (Fig. S18c).

The oxygen reduction abilities of the catalysts were further tested by the oxygen reduction reaction (ORR), and the performance of each carbon nitride is shown in Fig. 4e. The cyclic voltammetry (CV) curves of our catalyst were collected in N_2 and O_2 saturated 0.1 M KOH solutions with a scan rate of 50 mVs⁻¹. As shown in Fig. 4e, no discernible features were displayed in N_2 saturated solution, implying that no reaction occurs in that reaction condition. For the O_2 saturated solution a pronounced oxygen reduction peak appearing at approximately -0.36 V vs. Ag/AgCl was observed, suggesting that this catalyst can significantly catalyze the oxygen reduction reaction. The linear scan voltammetry (LSV) was measured on a rotating disk electrode (RDE) in the above O_2 saturated solution at 1600 rpm. As shown in Fig. S19 for TCNS and CNS the onset potential and half-wave potential of the ORR are basically consistent but prior to CN, suggesting that the TCNS and CNS have a better ability to reduce oxygen. TCNS has a slightly larger current density (inset of Fig. S19) than CNS and may result in slightly better activity than CNS.

TCNS also presented a high conversion activity and a high selectivity for the conversion of benzylamine derivatives (electron donating groups $-CH_3$ and CH_3O- , electron withdrawing group $-Cl$ and $-F$) to produce the corresponding imines (Fig. 4f). These substituents have a slight influence on the reaction conversion and product selectivity. Benzaldehyde was detected using GC-MS, which implies that the phenethylamine converts to 1-phenyl-N-(2-phenylethyl) methanimine (PEA) via a condensation reaction with benzaldehyde. It is deduced that the special structure of benzylamine, i.e., the existence of the benzyl group, is favored for the reaction. As the oxidation of benzylamine first forms a N radical under irradiation, then an electron transfer from the N atom to the adjacent C atom creates a stable C radical due to the stability in the presence of the benzene ring [59]. The activated benzylamine reacts with active oxygen to produce the benzaldehyde intermediate. Then, benzaldehyde reacts with benzylamine to form imine via a condensation reaction. TCNS exhibited good recyclability and the conversion rate remained above 91% after four successive reaction cycles (Fig. S20). TCNS was collected after each reaction cycle and measured using various techniques including XRD, FT-IR and UV-vis spectroscopy (Fig. S21a–c). According to the XRD, FT-IR and UV-vis spectra, no obvious structure change was observed after each reaction cycle. This demonstrate the chemically stable of our catalyst.

Based on the above analysis, a reaction mechanism was proposed (Fig. 4g). The introduction of a cyano group in C_3N_4 enhances the photoactivity primarily in two ways. First, the electronegative N atoms reduces the electron density of C atoms and polarizes the C atoms into C ($\delta+$), making it easy for adsorption of the O_2 atoms [63]. The sp hybrid structure of the $-C\equiv N$ group own higher electronegativity than the sp^2 hybrid orbital structure, thus the C atoms in $-C\equiv N$ group is more polarizes ($\delta++$) than the original structure. Furthermore, the effect of $-C\equiv N$ groups modification resembles n-doping, there are more non-paired electrons in the $-C\equiv N$ group modification sample, and the non-paired electrons can act as free electrons to participate in the photo-excitation process. It was reported that for water splitting the reduction and oxidation sites occur independently in the carbon and nitrogen atoms [8]. Due to the holes generated at the N atoms and the electrons generated at C atoms, the free electrons can be captured by the absorbed O_2 and produce the O_2^{+} radicals. Meanwhile, the amine was captured by the N atom to form the surface complex (Fig. S22), and preliminarily oxidized by the hole and lost an electron. Then, it was abstracted of a proton and a hydrogen atom by the O_2^{+} radical anion

to form a carbocationic-radical type intermediate, and subsequently generated benzaldehyde. The benzaldehyde can couple with other amines and undergo hole-assisted elimination of H_2O to afford the final coupled product.

4. Conclusions

In conclusion, we have introduced $-C\equiv N$ groups into the CN heterocycle structure. The effect of $-C\equiv N$ groups modification was similar to that of n-doping and can tune the optical properties and electronic band structure of carbon nitride. The obtained CNS and TCNS shows a lower recombination rate of photoinduced carriers. The terminal $-C\equiv N$ groups can tune the original connection pattern of C_3N_4 , which is beneficial for post thermal stripping. Sample TCNS achieves a thinner structure, which favors the photogenerated carrier transfer from the bulk to the surface. Furthermore, this catalyst exhibits excellent stability in cyclic tests and well tolerates the alteration of amine derivatives. This work opens new vistas for modifying carbon nitride. The group introduction method is a promising approach to improving the catalytic performance of carbon nitride. Whether other groups such as the $-C\equiv CH$ group hold the same performance is still being researched.

Acknowledgments

This work was supported by the National Natural Science Foundation of China (Nos. 21773284, 21503258), the Shanxi Science and Technology Department (Nos. 2015081044, 201601D021032), the Foundation of State Key Laboratory of Coal Conversion (No. J17-18-605), and the Hundred Talents Programs of the Chinese Academy of Sciences and Shanxi Province.

Appendix A. Supplementary data

Supplementary material related to this article can be found, in the online version, at doi:<https://doi.org/10.1016/j.apcatb.2018.09.084>.

References

- [1] H. Zhu, X. Ke, X. Yang, S. Sarina, H. Liu, Angew. Chem. Int. Ed. 49 (2010) 9657–9661.
- [2] I. Ghosh, T. Ghosh, J.I. Bardagi, B. Koenig, Science 346 (2014) 725–728.
- [3] J. Liu, Y. Liu, N. Liu, Y. Han, X. Zhang, H. Huang, Y. Lifshitz, S.-T. Lee, J. Zhong, Z. Kang, Science 347 (2015) 970–974.
- [4] A. Fujishima, Nature 238 (1972) 37–38.
- [5] J. Yu, J. Ran, Energy Environ. Sci. 4 (2011) 1364–1371.
- [6] C. Huang, C. Chen, M. Zhang, L. Lin, X. Ye, S. Lin, M. Antonietti, X. Wang, Nat. Commun. 6 (2015) 7698.
- [7] P. Yang, J. Zhao, W. Qiao, L. Li, Z. Zhu, Nanoscale 7 (2015) 18887–18890.
- [8] X. Wang, K. Maeda, A. Thomas, K. Takanabe, G. Xin, J.M. Carlsson, K. Domen, M. Antonietti, Nat. Mater. 8 (2009) 76–80.
- [9] K. Wang, Q. Li, B. Liu, B. Cheng, W. Ho, J. Yu, Appl. Catal. B: Environ. 176 (2015) 44–52.
- [10] T. Sano, S. Tsutsui, K. Koike, T. Hirakawa, Y. Teramoto, N. Negishi, K. Takeuchi, J. Mater. Chem. A 1 (2013) 6489–6496.
- [11] F. Goettmann, A. Fischer, M. Antonietti, A. Thomas, Angew. Chem. Int. Ed. 45 (2006) 4467–4471.
- [12] F. Su, S.C. Mathew, L. Moehlmann, M. Antonietti, X. Wang, S. Blechert, Angew. Chem. Int. Ed. 50 (2011) 657–660.
- [13] F. Su, S.C. Mathew, G. Lipner, X. Fu, M. Antonietti, S. Blechert, X. Wang, J. Am. Chem. Soc. 132 (2010) 16299–16301.
- [14] J. Ran, T.Y. Ma, G. Gao, X.-W. Du, S.Z. Qiao, Energy Environ. Sci. 8 (2015) 3708–3717.
- [15] J. Zhang, Y. Chen, X. Wang, Energy Environ. Sci. 8 (2015) 3092–3108.
- [16] J.K. Nørskov, T. Bligaard, J. Rossmeisl, C.H. Christensen, Nat. Chem. 1 (2009) 37–46.
- [17] C. Tang, Q. Zhang, Adv. Mater. 29 (2017) 1604103–1604111.
- [18] X. Wang, X. Chen, A. Thomas, X. Fu, M. Antonietti, Adv. Mater. 21 (2009) 1609–1612.
- [19] G. Zhang, M. Zhang, X. Ye, X. Qiu, S. Lin, X. Wang, Adv. Mater. 26 (2014) 805–809.
- [20] G. Liu, P. Niu, C. Sun, S.C. Smith, Z. Chen, G.Q. Lu, H.-M. Cheng, J. Am. Chem. Soc. 132 (2010) 11642–11648.
- [21] M. Shalom, S. Inal, C. Fettkenhauer, D. Neher, M. Antonietti, J. Am. Chem. Soc. 135 (2013) 7118–7121.
- [22] J. Zhang, X. Chen, K. Takanabe, K. Maeda, K. Domen, J.D. Epping, X. Fu,

- M. Antonietti, X. Wang, Angew. Chem. Int. Ed. 49 (2010) 441–444.
- [23] J. Hong, X. Xia, Y. Wang, R. Xu, J. Mater. Chem. 22 (2012) 15006–15012.
- [24] J. Zhang, M. Zhang, R.Q. Sun, X. Wang, Angew. Chem. Int. Ed. 124 (2012) 10292–10296.
- [25] F. Dong, Z. Zhao, T. Xiong, Z. Ni, W. Zhang, Y. Sun, W.-K. Ho, ACS Appl. Mater. Interface 5 (2013) 11392–11401.
- [26] E. Cheng, W. Yin, S. Bai, R. Qiao, Y. Zhong, Z. Li, Mater. Lett. 146 (2015) 87–90.
- [27] P. Niu, L. Zhang, G. Liu, H.M. Cheng, Adv. Funct. Mater. 22 (2012) 4763–4770.
- [28] Q. Lin, L. Li, S. Liang, M. Liu, J. Bi, L. Wu, Appl. Catal. B: Environ. 163 (2015) 135–142.
- [29] I.-Y. Jeon, H.-J. Choi, M. Choi, J.-M. Seo, S.-M. Jung, M.-J. Kim, S. Zhang, L. Zhang, Z. Xia, L. Dai, Sci. Rep. 3 (2013).
- [30] V.W.-h. Lau, I. Moudrakovski, T. Botari, S. Weinberger, M.B. Mesch, V. Duppel, J. Senker, V. Blum, B.V. Lotsch, Nat. Commun. 7 (2016) 12165.
- [31] X. Lang, H. Ji, C. Chen, W. Ma, J. Zhao, Angew. Chem. Int. Ed. 50 (2011) 3934–3937.
- [32] S. Silva, G. Amaralunga, Thin Solid Films 270 (1995) 194–199.
- [33] C. Chen, J. Robertson, Carbon 37 (1999) 839–842.
- [34] S. Silva, J. Robertson, G. Amaralunga, B. Rafferty, L. Brown, J. Schwan, D. Franceschini, G. Mariotto, J. Appl. Phys. 81 (1997) 2626–2634.
- [35] M.J. Frisch, G.W. Trucks, H.B. Schlegel, G.E. Scuseria, M.A. Robb, J.R. Cheeseman, G. Scalmani, V. Barone, G.A. Petersson, H. Nakatsuji, X. Li, M. Caricato, A.V. Marenich, J. Bloino, B.G. Janesko, R. Gomperts, B. Mennucci, H.P. Hratchian, J.V. Ortiz, A.F. Izmaylov, J.L. Sonnenberg, F. Williams, F. Ding, F. Lipparini, J. Egidi, B. Goings, A. Peng, T. Petrone, D. Henderson, V.G. Ranasinghe, J. Zakrzewski, N. Gao, G. Rega, W. Zheng, M. Liang, M. Hada, K. Ehara, R. Toyota, J. Fukuda, M. Hasegawa, T. Ishida, Y. Nakajima, O. Honda, H. Kitao, T. Nakai, K. Vreven, J.A. Throssell, J.E. Montgomery Jr., F. Peralta, M.J. Ogliaro, J.J. Bearpark, E.N. Heyd, K.N. Brothers, V.N. Kudin, T.A. Staroverov, R. Keith, J. Kobayashi, K. Normand, A.P. Raghavachari, J.C. Rendell, S.S. Burant, J. Iyengar, M. Tomasi, J.M. Cossi, M. Millam, C. Klene, R. Adamo, J.W. Cammi, R.L. Ochterski, K. Martin, O. Morokuma, J.B. Farkas, D.J. Foresman, Fox, Gaussian 09, Wallingford, CT (2009).
- [36] Y. Chen, B. Wang, S. Lin, Y. Zhang, X. Wang, J. Phys. Chem. C 118 (2014) 29981–29989.
- [37] M.J. Bojdys, J.O. Müller, M. Antonietti, A. Thomas, Chem.—Eur. J. 14 (2008) 8177–8182.
- [38] J. Zhang, M. Zhang, G. Zhang, X. Wang, ACS Catal. 2 (2012) 940–948.
- [39] X.L. Wang, W.Q. Fang, H.F. Wang, H. Zhang, H. Zhao, Y. Yao, H.G. Yang, J. Mater. Chem. A 1 (2013) 14089–14096.
- [40] S. Kumar, T. Tansley, Thin Solid Films 256 (1995) 44–47.
- [41] B. Bouchet-Fabre, K. Zellama, C. Godet, D. Ballutaud, T. Minéa, Thin Solid Films 482 (2005) 156–166.
- [42] A. Majumdar, G. Scholz, R. Hippel, Surf. Coat. Technol. 203 (2009) 2013–2016.
- [43] S. Kennou, S. Logothetidis, L. Sygellou, A. Laskarakis, D. Sotiropoulou, Y. Panayiotatos, Diamond Relat. Mater. 11 (2002) 1183–1187.
- [44] Y. Gui, J. Zhang, G. Zhang, J. Huang, P. Liu, M. Antonietti, X. Wang, J. Mater. Chem. 21 (2011) 13032–13039.
- [45] C. Baddiel, G. Janz, Trans. Faraday Soc. 60 (1964) 2009–2012.
- [46] T. Barakat, M. Nelson, S. Nelson, A. Pullin, Trans. Faraday Soc. 62 (1966) 2674–2684.
- [47] J. Zhang, M. Zhang, L. Lin, X. Wang, Angew. Chem. 127 (2015) 6395–6399.
- [48] J. Zhang, J. Sun, K. Maeda, K. Domen, P. Liu, M. Antonietti, X. Fu, X. Wang, Energy Environ. Sci. 4 (2011) 675–678.
- [49] Y. Kang, Y. Yang, L.-C. Yin, X. Kang, L. Wang, G. Liu, H.-M. Cheng, Adv. Mater. 28 (2016) 6471–6477.
- [50] L. Shi, K. Chang, H. Zhang, X. Hai, L. Yang, T. Wang, J. Ye, Small 12 (2016) 4431–4439.
- [51] L.-W. Ruan, Y.-J. Zhu, L.-G. Qiu, Y.-P. Yuan, Y.-X. Lu, Comput. Mater. Sci. 91 (2014) 258–265.
- [52] J. Cheng, Z. Hu, K. Lv, X. Wu, Q. Li, Y. Li, X. Li, J. Sun, Appl. Catal. B: Environ. 232 (2018) 330–339.
- [53] H. Yaghoubi, Z. Li, Y. Chen, H.T. Ngo, V.R. Bhethanabotla, B. Joseph, S. Ma, R. Schlaf, A. Takshi, ACS Catal. 5 (2014) 327–335.
- [54] J. Zhang, M. Zhang, L. Lin, X. Wang, Angew. Chem. Int. Ed. 54 (2015) 6297–6301.
- [55] J. Xu, Y. Wang, Y. Zhu, Langmuir 29 (2013) 10566–10572.
- [56] N. Zhang, X. Li, H. Ye, S. Chen, H. Ju, D. Liu, Y. Lin, W. Ye, C. Wang, Q. Xu, J. Zhu, L. Song, J. Jiang, Y. Xiong, J. Am. Chem. Soc. 138 (2016) 8928–8935.
- [57] S.E. Diamond, G.M. Tom, H. Taube, J. Am. Chem. Soc. 97 (1975) 2661–2664.
- [58] M. Tabbal, T. Christidis, S. Isber, P. Mérél, M.A. El Khakani, M. Chaker, A. Amassian, L. Martinu, J. Appl. Phys. 98 (2005) 044310.
- [59] Y. Zhang, L. Pei, Z. Zheng, Y. Yuan, T. Xie, J. Yang, S. Chen, J. Wang, E.R. Wacławik, H. Zhu, J. Mater. Chem. A 3 (2015) 18045–18052.
- [60] P. Christopher, H. Xin, S. Linic, Nature Chem. 3 (2011) 467–472.
- [61] D. Brinkley, T. Engel, J. Phys. Chem. B 104 (2000) 9836–9841.
- [62] X. Guo, C. Hao, G. Jin, H. Zhu, X. Guo, Angew. Chem. Int. Ed. 53 (2014) 1973–1977.
- [63] Z. Luo, S. Lim, Z. Tian, J. Shang, L. Lai, B. MacDonald, C. Fu, Z. Shen, T. Yu, J. Lin, J. Mater. Chem. 21 (2011) 8038–8044.